Geophysical Research Letters

RESEARCH LETTER
10.1029/2022GL100719

Key Points:

- A pathway of three coupled ocean-atmosphere feedbacks communicates extratropical anomalous cooling and sustains a tropical response
- Broadly, buoyancy-forced adjustments dominate in the subtropics while momentum-forced adjustments create zonal asymmetries in the tropics
- This mechanistic pathway seems to be robust across several global climate models

Supporting Information:

Supporting Information may be found in the online version of this article.

Correspondence to:

M. T. Luongo,
mluongo@ucsd.edu

Citation:

Luongo, M. T., Xie, S.-P., Eisenman, I., Hwang, Y.-T., & Tseng, H.-Y. (2023). A pathway for northern hemisphere extratropical cooling to elicit a tropical response. *Geophysical Research Letters*, *50*, e2022GL100719. https://doi.org/10.1029/2022GL100719

Received 10 AUG 2022
Accepted 29 DEC 2022

A Pathway for Northern Hemisphere Extratropical Cooling to Elicit a Tropical Response

Matthew T. Luongo[1], Shang-Ping Xie[1], Ian Eisenman[1], Yen-Ting Hwang[2], and Hung-Yi Tseng[2]

[1]Scripps Institution of Oceanography, University of California San Diego, La Jolla, CA, USA, [2]Department of Atmospheric Sciences, National Taiwan University, Taipei, Taiwan

Abstract Previous studies have found that Northern Hemisphere aerosol-like cooling induces a La Niña-like response in the tropical Indo-Pacific. Here, we explore how a coupled ocean-atmosphere feedback pathway communicates and sustains this response. We override ocean surface wind stress in a comprehensive climate model to decompose the total ocean-atmosphere response to forced extratropical cooling into the response of surface buoyancy forcing alone and surface momentum forcing alone. In the subtropics, the buoyancy-forced response dominates: the positive low cloud feedback amplifies sea surface temperature (SST) anomalies which wind-driven evaporative cooling communicates to the tropics. In the equatorial Indo-Pacific, buoyancy-forced ocean dynamics cool the surface while the Bjerknes feedback creates zonally asymmetric SST patterns. Although subtropical cloud feedbacks are model-dependent, our results suggest this feedback pathway is robust across a suite of models such that models with a stronger subtropical low cloud response exhibit a stronger La Niña response.

Plain Language Summary Anthropogenic aerosols are an important radiative forcing on the climate system contributing to observed climate variability. In prior modeling studies, idealized aerosol-like forcing applied to Northern Hemisphere high latitude regions has resulted in a tropical La Niña-like response in the Eastern Equatorial Pacific. In this study, we investigate the pathway by which high latitude aerosol-like cooling is communicated to the tropics via a sequence of ocean-atmosphere positive feedback processes. We explore this pathway further by parsing out the total climate response into surface forcing which alters the buoyancy of seawater via heat or freshwater and surface wind stress forcing which alters the momentum of seawater. We find that subtropical patterns, arising from low clouds and wind-induced evaporative cooling, are primarily buoyancy-forced, while tropical asymmetries arise from momentum forcing. The results show that this pathway is robust across seven climate models such that stronger subtropical cloud responses elicit stronger sea surface temperature responses in the equatorial Pacific. The results highlight the important link between extratropical aerosol-like forcing and La Niña-like patterns via these coupled ocean-atmosphere feedbacks. The equatorial Pacific can drive major climate variability, suggesting global implications for these results.

1. Introduction

Extratropical atmospheric variability, either resulting from internal climate variability (e.g., Chang et al., 2007; Hasselmann, 1976) or in response to an anomalous forcing of the climate system (e.g., Hwang et al., 2017; Kang et al., 2008), can influence the tropics through coupled ocean-atmosphere interactions. Due to the global influence of the El Niño-Southern Oscillation (ENSO), extratropical forcing of ENSO variability is of particular interest. Many studies (e.g., Chang et al., 2007; Larson & Kirtman, 2013, 2014; Lu et al., 2017; Ma et al., 2017; Pegion & Selman, 2017; E. E. Thomas & Vimont, 2016; Vimont et al., 2003) have shown that variations in the Pacific Meridional Mode (PMM: Amaya, 2019; Chiang & Vimont, 2004), the second leading mode of North Pacific ocean-atmosphere variability, can communicate extratropical variability to the tropics via the Wind-Evaporation-Sea Surface Temperature (WES: Xie & Philander, 1994) feedback. This stochastic extratropical forcing on the tropics may then excite the tropical Bjerknes feedback (Bjerknes, 1969) and develop into an El Niño or La Niña event.

In addition to interannual extratropical forcing (Nonaka et al., 2000, 2002), factors which have been shown to elicit tropical responses include sustained extratropical forcing from idealized perturbations (Kang et al., 2008, 2009), ocean thermohaline circulation changes (Dong & Sutton, 2002; R. Zhang & Delworth, 2005), sea ice changes (Chiang & Bitz, 2005; Mahajan et al., 2011), and aerosol forcing (Verma et al., 2019; Yoshimori & Broccoli, 2008).

The Extratropical-Tropical Interaction Model Intercomparison Project (ETINMIP: Kang et al., 2019) builds on this work and seeks to understand the dynamic linkages between extratropical forcing and subsequent tropical responses in realistic coupled global climate models (GCMs). In ETINMIP, a zonally uniform reduction in top-of-atmosphere (TOA) solar insolation is continuously applied to multiple GCMs in either the Northern Hemisphere (NH) or Southern Hemisphere (SH) extratropics. In the equatorial Pacific Ocean, a La Niña-like sea surface temperature (SST) pattern is a robust response across models in the long-term, multi-model mean under both the NH and SH ETINMIP forcing (Kang et al., 2019, 2020).

While several studies have used atmospheric GCMs thermodynamically coupled to motionless slab ocean models to suggest an idealized surface pathway of WES-driven extratropical forcing of the tropics (Hsiao et al., 2022; Hwang et al., 2017; Kang et al., 2014, 2020), Kang et al. (2020) show that the La Niña-like response to NH extratropical forcing is only present when the ocean is allowed to dynamically adjust. They explain this difference by suggesting that cooled subtropical waters upwell in the Eastern Equatorial Pacific (EEP) via the climatological subtropical cells (STCs: McCreary & Lu, 1994; Z. Liu, 1994) and that these cooler waters then create a zonal gradient in SST via the Bjerknes feedback. This subsurface pathway (Burls et al., 2017; Heede et al., 2020; Z. Liu & Huang, 1997; E. E. Thomas & Vimont, 2016) is one conduit by which extratropical variability influences the tropics (England et al., 2020; Luongo et al., 2022; Stuecker et al., 2020; Vannière et al., 2014; Wang et al., 2018). However, despite a strong subtropical atmospheric response, Y. Zhang et al. (2021) show that equatorial SST variability is suppressed in the presence of mean equatorial upwelling alone, suggesting the importance of surface processes in inducing and sustaining a forced tropical response.

Although the subsurface adjustments may provide the initial cooling needed to create the La Niña-like quasi-equilibrium response, these discussions ignore an important kinematic spatial pathway of coupled surface ocean-atmosphere processes which amplify and maintain the decadal to centennial response of the tropical Indo-Pacific to aerosol-like forcing. In this study we explore a pathway by which three coupled feedback processes, the low cloud-SST, WES, and Bjerknes feedbacks, communicate NH extratropical cooling to the tropical Pacific and sustain a La Niña-like quasi-equilibrium response. We employ a series of wind stress locking experiments from Luongo et al. (2022) to partition the ocean's fully coupled response into buoyancy-forced and momentum-forced adjustments. We show that the subtropics are dominated by buoyancy-forced modes (Section 3.1), while zonal tropical modes are momentum-forced (Section 3.2). We discuss what these wind stress locking simulations imply for tropical mode phase estimation (Section 4.1) and the extent to which the proposed coupled process pathway is robust across ETINMIP member models (Section 4.2). We conclude in Section 5.

2. Experimental Design and Methods

2.1. GCM Simulations

We use the output from five experiments carried out with version 1.2.2 of the Community Earth System Model (CESM: Hurrell et al., 2013) in a standard, coupled pre-industrial configuration with atmosphere and land components run on a nominally 2° horizontal resolution and ocean and sea ice components run on a nominally 1° horizontal resolution. We force CESM with a hemispherically asymmetric aerosol-like radiative forcing by abruptly reducing TOA solar insolation from 45–65°N following the ETINMIP NH Extratropical forcing protocol (Figure S1 in Supporting Information S1). This forcing corresponds to an annual-mean, zonal-mean forcing of approximately -45 Wm^{-2} at 55°N, or about -1.6 Wm^{-2} globally averaged.

To decompose the ocean's total response into surface buoyancy forcing alone and surface momentum forcing alone, we output daily wind stress from a freely evolving unforced pre-industrial control case (Clim1) and an NH ETINMIP forcing case (Clim2). We then globally override surface ocean wind stress at each daily coupling step in three experiments: an unforced case where wind stress is prescribed from Clim1 but offset by a year (Tau1S1, our mechanically decoupled control), an NH ETINMIP forced experiment with unforced wind stress from Clim1 (Tau1S2), and an experiment without radiative forcing but with forced wind stress prescribed from Clim2 (Tau2S1). We approximate the ocean's total response to this aerosol-like TOA insolation reduction (fully coupled: FC = Clim2-Clim1) as the linear sum of the ocean's response to the change in surface buoyancy forcing (buoyancy-forced: BF = Tau1S2-Tau1S1) and the ocean's response to the change in surface wind stress forcing (momentum-forced: MF = Tau2S1-Tau1S1):

$$\mathrm{FC} \approx \mathrm{BF} + \mathrm{MF}\,. \tag{1}$$

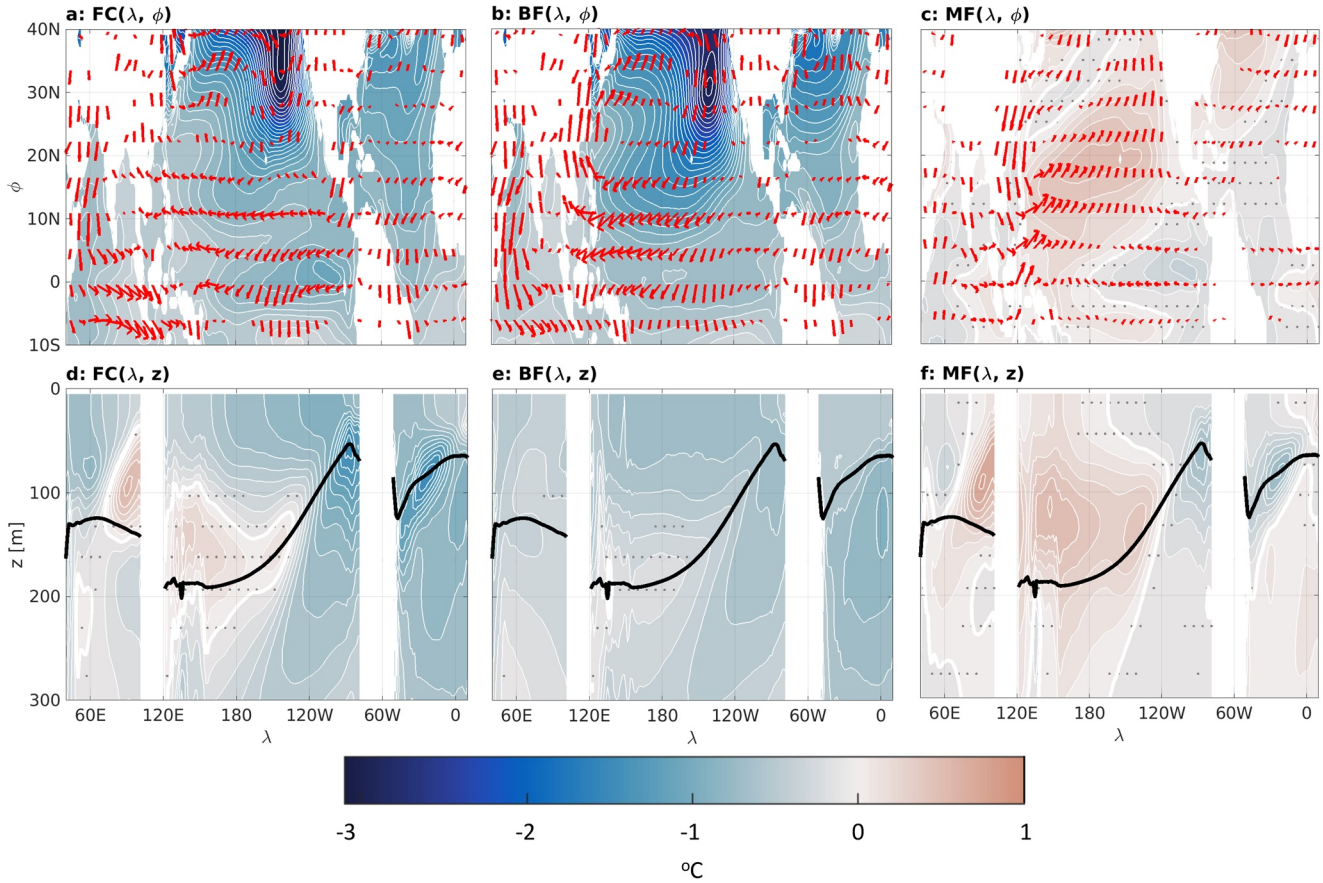

Figure 1. Top row: Sea surface temperature (colorfill and white contours) for FC (a), BF (b), and MF (c) with 850 hPa near-surface wind vectors. Bottom row: Equatorial (averaged over 5°S–5°N) temperature depth-profile (colorfill and white contours) for FC (d), BF (e), and MF (f). In all plots, temperature has contours of 0.1°C and the zero contour is plotted as a thick white line. Decadal average temperature responses which are not signficant at the 90% confidence level using a two-sided Student T-test are stippled. In the bottom row, the $\sigma_0 = 25$ kg m^{-3} isopycnal of the control simulation is plotted as a thick black line.

By overriding wind stress, we build on prior studies which have mechanically decoupled the ocean from the atmosphere through wind stress overriding (e.g., Gregory et al., 2016; Larson et al., 2018; W. Liu et al., 2018; Luongo et al., 2022). While overriding wind stress and mechanically decoupling the ocean and atmosphere inevitably influences the climate, Luongo et al. (2022) show that these decoupling nonlinearities are small compared to the forced responses. We emphasize that our protocol overrides surface wind stress rather than total wind: MF isolates the Ekman adjustment, while wind speed effects [e.g., for turbulent heat fluxes as overridden by Mahajan et al. (2009) or Smirnov and Vimont (2012)] are retained within BF. To minimize the effects of internal variability within CESM, we run three realizations of each of these five cases with slightly different initial conditions (Kay et al., 2015) and present the ensemble mean of the three realizations throughout this study. Lastly, as we are interested in the quasi-steady state response of the ocean-atmosphere system in this paper, we focus on the average of the last 40 years of the 50-year simulations. Because these 40-year averaged SST patterns (Figure 1) agree well with the "long-term" (100–150 year average, Figure S2 in Supporting Information S1) response of CESM to NH ETINMIP forcing, we consider this the quasi-equilibrium response of the surface ocean. See Table S1 in Supporting Information S1 or Luongo et al. (2022) for further simulation details.

2.2. Ocean Mixed Layer Heat Budget

To attribute the dynamic drivers of specific SST patterns, we perform an energy budget analysis of the ocean mixed layer (e.g., Hwang et al., 2017; Xie et al., 2010):

$$\rho_0 C_p H \frac{\partial T}{\partial t} = Q'_{net} + D'_o = Q'_{SW} + Q'_{LW} + Q'_{SH} + Q'_{LH} + D'_o \,. \quad (2)$$

Above, the left-hand side is the product of seawater density (ρ_0, assumed to be constant), ocean heat capacity (C_p), mixed layer depth (H), and temperature tendency ($\partial T/\partial t$). The right-hand side is the sum of net surface heat flux perturbations, Q'_{net}, and horizontal divergence of three-dimensional ocean heat transport, D'_o, which includes advective and diffusive processes. Because $\partial T/\partial t$ is near zero in the quasi-equilibrium tropics and subtropics, this implies that the change in Q'_{net}, which is the sum of changes in shortwave $\left(Q'_{SW}\right)$, longwave $\left(Q'_{LW}\right)$, sensible $\left(Q'_{SH}\right)$, and latent heat fluxes $\left(Q'_{LH}\right)$, is approximately balanced by D'_o.

Based on the linear bulk formulation for evaporation, which dominates latent heat flux changes in the tropics and subtropics (i.e., $Q'_{LH} \approx -Q'_E$: see Figure S3 in Supporting Information S1), we decompose latent heat flux changes into changes from variations in wind speed (W), relative humidity (RH), air-sea temperature gradient (S), and a Newtonian cooling term proportional to the SST anomaly. By normalizing by the product of the mean evaporative heat flux and a Clausius-Clapeyron scaling, we write a diagnostic equation for SST anomalies:

$$T' = T'_{SW} + T'_{LW} + T'_{SH} + T'_{E,W} + T'_{E,RH} + T'_{E,S} + T'_{Do} \approx T'_R + T'_E + T'_{Do}\,. \tag{3}$$

This decomposition allows us to diagnose the primary drivers of SST anomalies in specific regions (Figure S4 in Supporting Information S1) and identify leading dynamic modes of variability. Noting that tropical and subtropical sensible heat fluxes are small ($T'_{SH} \approx 0$, Figures S3 and S4 in Supporting Information S1), we approximate the full decomposition as a sum of the radiative terms ($T'_R = T'_{SW} + T'_{LW}$, primarily driven by T'_{SW}), T'_{Do}, and the evaporative terms ($T'_E = T'_{E,W} + T'_{E,RH} + T'_{E,S}$, driven primarily by $T'_{E,W}$). See Text S1 in Supporting Information S1 for a detailed derivation of Equation 3.

3. Extratropical-Tropical Pathway

3.1. Buoyancy-Dominated Subtropics

Striking similarities in SST and near-surface wind patterns exist between the FC and BF Pacific and Atlantic NH subtropics (Figures 1a and 1b). These similarities emphasize the extent to which buoyancy forcing dominates the total subtropical response of the ocean-atmosphere system. In the Pacific basin, a strong zonal SST gradient develops such that the eastern half of the basin is significantly cooler than the western half; SST perturbations are most highly negative below the marine stratiform cloud deck off the west coast of North America. In the marine stratocumulus regime, the positive low cloud feedback (Clement et al., 2009; Hsiao et al., 2022; Norris & Leovy, 1994; Norris et al., 1998; Wood, 2012; Yang et al., 2022) can amplify negative SST perturbations by increasing cloud cover, reducing solar insolation, and cooling local SSTs further. Figure S9 of Luongo et al. (2022) demonstrates CESM's strong increase in low cloud cover and subsequent decrease in surface shortwave radiative forcing in both FC and BF; this decrease in solar forcing coincides with the amplified negative SST anomalies in the northeast subtropical Pacific seen in Figures 1a and 1b. We diagnostically attribute this cooling to the cloud cover increase through the mixed layer budget decomposition: Figure 2a shows that radiative forcing $\left(T'_R\right)$, dominated by T'_{SW}, is the primary driver of total temperature change (T'). The low cloud driven shortwave radiative forcing effect drives negative SST anomalies in the Northeast Pacific low cloud deck, although wind speed driven changes $\left(T'_E\right)$ also contribute to negative SST anomalies, whereas ocean heat transport $\left(T'_{Do}\right)$ acts to warm SST.

In both FC and BF, these SST anomalies extend southwestward from the low cloud deck and resemble the familiar PMM pattern (Amaya, 2019; Chiang & Vimont, 2004), which propagates negative SST anomalies southwestward via the WES feedback (Xie, 1999). These PMM patterns are accompanied by basin-scale anti-cyclonic anomalous near-surface winds. Figure 2b shows that the PMM-like cooling observed in the subtropical western Pacific in FC and BF is driven by thermodynamic effects of wind speed on latent heat flux. While other factors influence this region's total SST change, wind speed, and thus the WES feedback, is the largest driver of negative SST anomalies in the subtropical western Pacific where this PMM propagates. The fact that this cooling is communicated southwestward via a PMM is significant as these PMM winds can force the tropics with extratropical variability. This agreement between FC and BF is in marked contrast to the MF case, which largely diverges from the FC response: momentum-forced adjustment leads to subtropical SST warming in both the Pacific and Atlantic basins (Figure 1c). In particular, Ekman adjustments act as a negative feedback on WES-driven cooling (Kang et al., 2018; Xie, 1999) such that FC patterns resemble a weaker BF.

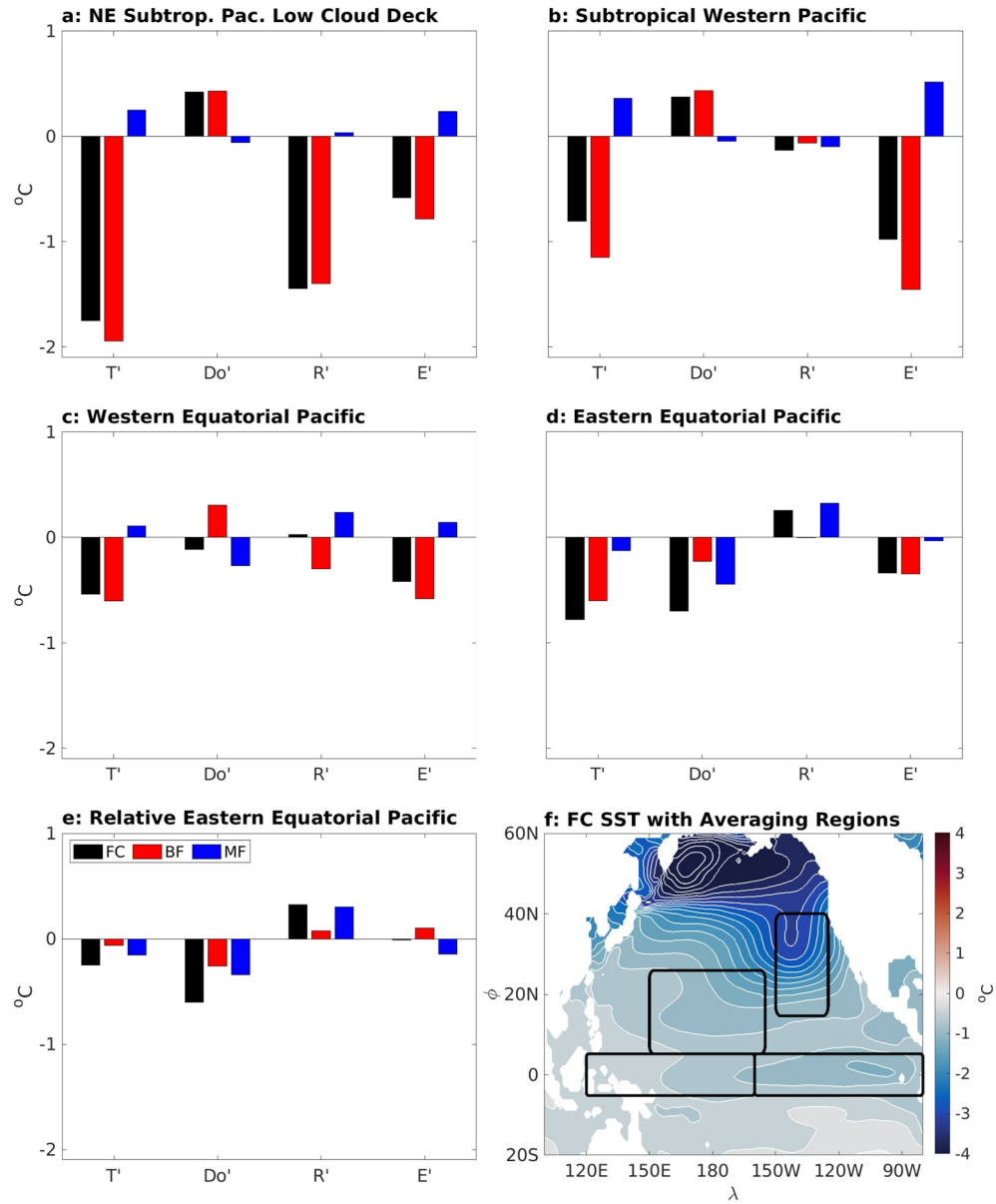

Figure 2. Ocean mixed layer sea surface temperature (SST) diagnostic attribution presented in Equation 3. Note that the "T'" on T'_{Do}, T'_R, and T'_E along the x-axis has been dropped for brevity. In panels (a–e), black bars are the FC response, red bars are the BF response, and blue bars are the MF response. These responses are averaged over respective regions of the Pacific ocean: the Northeast Pacific low cloud deck (15°N–40°N, 150°W–125°W) in panel (a), the subtropical western Pacific (5°N–25°N, 150°E–155°W) in panel (b), the Western Equatorial Pacific (5°S–5°N, 120°E–160°W) in panel (c), and the Eastern Equatorial Pacific (5°S–5°N, 160°W–80°W) in panel (d). The tropical average (20°S–20°N, 0°–360°) is subtracted from panel (d) to produce panel (e). Panel (f) shows the averaging regions over the FC SST response.

Though less coherent patterns exist in the Atlantic than the clear low cloud and PMM responses in the Pacific, the agreement between FC and BF subtropical Atlantic SST and near-surface wind is also strong. In both cases, cooling is concentrated in the western half of the basin and this cooling signal extends nearly into the tropics. Considered together, we conclude that buoyancy forcing dominates the subtropical NH response of the ocean adjustment and that the low cloud-SST and WES positive feedbacks act to cool the subtropics. The PMM then acts as a surface conduit by which extratropical cooling can then reach the tropics. We also note the strong similarity between subtropical BF cooling of SST from this low cloud-WES pathway with subtropical responses of motionless slab ocean models to similar forcing schemes (Hsiao et al., 2022; Hwang et al., 2017; Kang et al., 2014, 2020; Luongo et al., 2022).

3.2. Momentum-Driven Tropical Patterns

Though BF drives pattern formation in the subtropics and provides a large-scale surface cooling (Figure 1b), the La Niña and negative Indian Ocean Dipole (IOD) zonal SST dipoles present in the tropical FC response (Figure 1a) are clearly a result of MF-driven surface cooling in the EEP and the western equatorial Indian Ocean (Figure 1c). This image of MF-enabled tropical pattern formation becomes even more clear in the profiles of near-surface equatorial (average of 5°S–5°N) temperature presented in Figures 1d–1f. In FC, the Pacific and Indian basins feature strong zonal temperature dipoles: in the western Indian and EEP, cool temperature anomalies exist from the surface to depth (and well into the thermocline in the case of the Pacific), while the eastern Indian and Western Equatorial Pacific (WEP) are characterized by subsurface warm anomalies. These zonal dipoles present the so-called "tilt-mode" pattern in ENSO dynamics created by the Bjerknes feedback (e.g., Bunge & Clarke, 2014; Meinen & McPhaden, 2000; Wyrtki, 1975): changes in equatorial wind stress drive a tilting of the thermocline. Sure enough, comparison of the FC and MF profiles in Figures 1d and 1f confirms that the western Indian and EEP surface cooling and the eastern Indian and WEP subsurface warming so prominent in FC are statistically significant momentum-driven responses.

The BF temperature response exhibits interesting patterns which affect the FC response of the equatorial Pacific as well: the eastern Pacific is cooler at depth than the western Pacific. This subsurface cooling is likely a signature of buoyancy-forced STC adjustment (Burls et al., 2017; Heede et al., 2020; Kang et al., 2020; Z. Liu & Huang, 1997; Luongo et al., 2022). Verma et al. (2019) find that the initial response to hemispherically asymmetric aerosol forcing is a zonally asymmetric El Niño-like tropical Pacific SST response; this initial asymmetry is partially explained by the transient upwelling damping effect of the ocean dynamical thermostat (Clement et al., 1996; Heede & Fedorov, 2021). Continued upwelling likely works to erode this initial zonal asymmetry and cool the EEP and create the zonally symmetric BF mixed layer response (Figure 1e). However, while subsurface adjustments clearly affect the near-steady state response of the near surface equatorial Pacific, it is zonal asymmetries, as seen in MF, which set off the Bjerknes feedback.

Forced thermocline vertical displacements lead to surface temperature anomalies and our mixed layer decomposition allows us to diagnostically attribute the dynamic processes at play. WEP cooling (Figure 2c) largely follows the subtropical western Pacific: stronger wind speeds in BF increase evaporative cooling and primarily drive the total cooler FC response. In the EEP, however, different dynamics exist (Figure 2d). While the total T' response is still driven by BF (in large part from T'_E's evaporative cooling from increased trade winds), the T'_{Do} response associated with BF and MF plays an increased role in setting EEP SST. In the EEP, zonal currents, poleward meridional Ekman advection, and subsequent equatorial upwelling set climatological conditions, so it isn't necessarily surprising that ocean heat transport features prominently in the EEP's temperature response. Because strong BF evaporative cooling from the increased trade wind strength throughout the tropics obscures the local ocean adjustment in the EEP (Figures 1b and 2d), we consider the EEP response relative to the rest of the tropics. Following Kang et al. (2019, 2020), we subtract out the tropical mean (average of 20°S–20°N) response, of which the mean pattern is strongly a function of BF (not shown), to examine the EEP relative to the rest of the tropics (Figure 2e).

With this view, the total FC cooling is primarily a result of MF, specifically changes in ocean heat transport and increases in wind speed tempered by shortwave changes. To understand the zonal, meridional, and vertical ocean adjustment processes occurring in response to NH ETINMIP forcing, we perform an advective decomposition (e.g., Luongo et al., 2022; Wang et al., 2018; Yu & Pritchard, 2019) of ocean heat transport changes $\left(\vec{u}\cdot\nabla T = u\,\partial T/\partial x + v\,\partial T/\partial y + w\,\partial T/\partial z\right)$, integrated from the surface to 65 m depth (the average mixed layer depth in the control climate's EEP) and averaged over the EEP (Figure S6a in Supporting Information S1). Zonal changes from MF drive the EEP FC cooling response, a result of either altered currents or temperature gradients which potentially result from momentum-driven thermocline tilting. The meridional and vertical components of MF, which also cool, could result from the increased strength of the momentum-driven STC response (Green & Marshall, 2017; Luongo et al., 2022), which affects meridional heat divergence and upwelling strength. Though MF is the largest factor in relative EEP cooling, buoyancy-forced ocean heat transport changes, likely a result of STC adjustment (e.g., Burls et al., 2017; Z. Liu & Huang, 1997), also contribute to the cooling. However, Vannière et al. (2014) and M. D. Thomas and Fedorov (2017) show that subsurface adjustment mechanisms and time scales can vary across models: while Kang et al. (2020) suggest mean upwelling of cooler waters drives EEP cooling, stronger overturning and upwelling responses in a different GCM could drive this cooling as well

(e.g., Luongo et al., 2022). This mixed layer buoyancy-forced adjustment, and the subsurface adjustment seen in Figure 1b, merit further investigation.

4. Discussion

4.1. Tropical Mode Phase Estimation

In Section 3.2 we diagnose momentum forcing as the dominant driver of the Pacific Ocean La Niña pattern and Indian Ocean negative IOD pattern. However, a further question is why MF leads to negative phases of ENSO and IOD variability specifically. We make a simple argument based on momentum conservation. In Figure 1a, we see that FC τ^x is westward in the Central and WEP: easterly τ^x anomalies impart anomalous easterly momentum into the equatorial surface ocean. The ocean's adjustment to this anomalous easterly wind stress leads to a shoaling of the thermocline in EEP and a deepening of the thermocline in the WEP. Similarly, westerly τ^x anomalies over the eastern Indian Ocean lead to thermocline shoaling in the western Indian Ocean and thermocline deepening in the eastern Indian Ocean.

We can take this exercise one step further: why is τ^x easterly over WEP? Due to our wind stress locking methodology, τ^x in FC and MF are approximately equal. As discussed at length in Section 3.1, however, the subtropical FC response is driven nearly entirely by BF. We argue that the anomalous large-scale pattern of τ^x in FC, and by extension MF, is set by subtropical BF adjustment. The FC and BF responses of τ^x as calculated by CESM's atmospheric component (thus not affected by our wind stress overriding approach) exhibit a strong pattern correlation value of 0.774 (Figures S7a and S7b in Supporting Information S1), lending credence to our interpretation. In particular, the subtropical PMM pattern, seen so clearly in Figure 1b's near-surface wind field, serves as an extratropical boundary condition that provides momentum forcing to WEP in the FC response and leads to a La Niña-like SST response in EEP. The resulting strengthened Walker cell adjustment may then drive anomalous westerly τ^x over the Indian Ocean and lead to the negative IOD pattern. This recognition that subtropical BF provides a tropical input for MF is important: an understanding of large-scale BF patterns can lead to predictability of tropical MF modes. In a global warming analog, W. Liu et al. (2015) use an approximate wind stress locking method and similarly conclude that the IOD-like response to greenhouse forcing results from Bjerknes adjustment primed by WES forcing.

It's worth mentioning that this phase predictability does not seem to work well in the equatorial Atlantic. Sub-surface MF-driven cooling is present in the western tropical Atlantic (Figure 1f) in addition to a deeper eastern-basin intensified BF sub-surface cooling. While theoretically this pathway of three positive feedbacks (low cloud-SST, WES, and Bjerknes) could exist in the Atlantic basin, we see no sign of an Atlantic Niña in Figure 1c. This may be the result of well-known strong biases in the tropical Atlantic (e.g., Richter & Xie, 2008; Richter et al., 2012), the lack of a persistent subtropical low cloud deck off Africa's west coast, or the strength of natural variability in this region.

4.2. Robustness of Pathway Across ETINMIP

The magnitude of subtropical cloud feedbacks varies widely across GCMs (e.g., Forster et al., 2021; Zelinka et al., 2020). In this study, the proposed dynamic pathway which connects extratropical cooling with a tropical Indo-Pacific SST response occurs via three positive feedbacks: low cloud-SST and WES in the subtropics and Bjerknes in the deep tropics (schematically shown in Figure S8 in Supporting Information S1). Because this pathway involves cloud forcing, we might expect the response to be highly dependent on GCM choice. We test the robustness of this pathway across the seven ETINMIP member models by plotting the strength of the surface shortwave cloud radiative effect (SW CRE) in the northeast Pacific's low cloud deck, the Walker circulation index (defined as the difference between sea level pressure in the central/East Pacific, 160°–80°W, 5°S–5°N, and the Indian Ocean/west Pacific, 80°–160°E, 5°S–5°N: Kang et al., 2020), and the Nino 3.4 region (170°–120°W, 5°S–5°N) SST anomaly in Figures 3a and 3b. Strong, statistically significant correlations exist among the models between dynamically linked quantities, SW CRE and Walker cell strength and Nino3.4 SST and Walker cell strength; both relationships exhibit Pearson correlation coefficients of $|r| > 0.87$ ($p < 0.02$). Despite not being directly dynamically linked, the correlation between the starting point of our pathway, northeast Pacific low cloud deck SW CRE, and the endpoint, Nino3.4 SST, is also strong: $r = 0.759$ ($p < 0.05$). This correlation can be partially explained by the southward Intertropical Convergence Zone (ITCZ) shift and subsequent strengthening

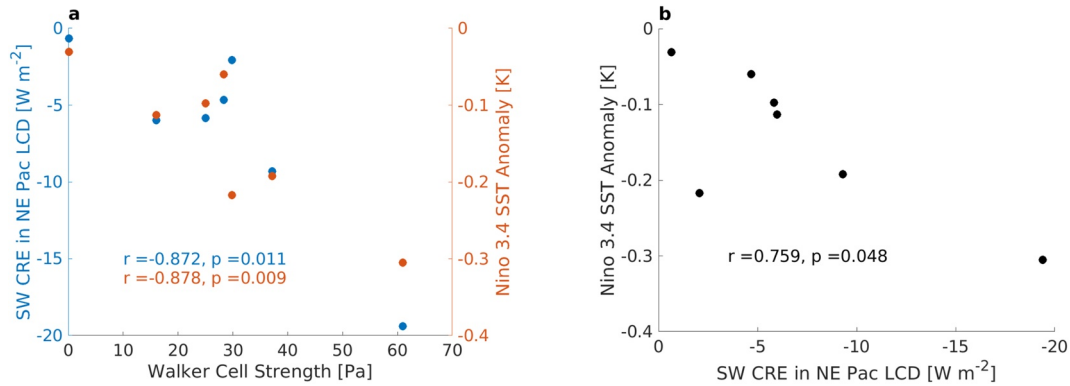

Figure 3. (a) Scatter plot of the surface shortwave cloud radiative effect (SW CRE) response among seven ETINMIP member models (blue dots) versus Walker circulation strength index, defined in Kang et al. (2020) as the sea level pressure difference over the Central/East Pacific (5°S–5°N, 160°W–80°W) and the Indian Ocean/West Pacific (5°S–5°N, 80°E−160°E), and scatter plot of the Nino3.4 region (5°S–5°N, 170°W–120°W) sea surface temperature (SST) response among seven ETINMIP member models (orange dots) versus Walker circulation strength index. (b) Scatter plot of SW CRE versus Nino3.4 SST response among seven ETINMIP member models (black dots).

of NH Hadley cell (Luongo et al., 2022) which would amplify low-cloud deck cover over the northeastern subtropical Pacific and reduce SSTs further.

Though the ETINMIP multi-model mean exhibits a La Niña-like response (Figure S9 in Supporting Information S1), a caveat to these correlations is that CESM exhibits far-and-away the strongest SW CRE, Walker cell strength, and Nino3.4 SST responses (furthest rightward dots in Figures 3a and 3b) and hence could be seen as driving this trend. Nevertheless, removing CESM still leads to a correlation of $r = -0.713$ between Walker cell strength and Nino3.4 SST response and $r = -0.662$ between Walker cell strength and SW CRE response, although the correlation between SW CRE and Nino3.4 SST drops to $r = 0.359$. All told, this suggests that this NH feedback pathway may be robust across ETINMIP member models: models with less of a SW CRE response in the northeast Pacific's marine stratiform regime exhibit less of a La Niña response in the EEP. This result is qualitatively similar to the results from two CESM cloud feedback sensitivity studies. Burls and Fedorov (2014) alter subtropical liquid water path in fully coupled CESM simulations and find a strong relationship between subtropical meridional cloud albedo gradient, Walker cell strength, and tropical Pacific zonal SST gradients. In addition, Erfani and Burls (2019) vary global cloud fraction under global warming forcing and find that ocean coupling allows for a stronger Walker response relative to the slab ocean model with the same cloud forcing.

5. Conclusions

In this study we have investigated a pathway by which coupled surface ocean-atmosphere feedbacks can communicate NH extratropical TOA cooling to the tropics and maintain a tropical near-steady state SST response. Our use of wind stress locked GCM simulations has allowed us to partition the ocean-atmosphere adjustment into buoyancy forcing alone and momentum forcing alone, and we then use an ocean mixed layer decomposition to diagnose and dynamically attribute SST responses in several key regions of the Indo-Pacific. We have found that buoyancy forcing largely dominates in the subtropical Pacific; in particular, the positive low cloud feedback creates strong SST anomalies in the northeast subtropical Pacific low cloud deck, and these anomalies are translated southwestward to the tropics via wind speed driven evaporative cooling (the WES feedback). This thermodynamically driven low cloud-WES mode response is qualitatively similar to simulations that use slab ocean models (e.g., Hsiao et al., 2022; Hwang et al., 2017; Kang et al., 2020). However, in dynamic ocean model simulations, these forced subtropical patterns provide an input to the tropics: anomalous easterlies in the WEP input anomalous easterly momentum to kick off the Bjerknes feedback in MF. This creates zonal SST dipoles in the Pacific and Indian Oceans: familiar La Niña and negative IOD patterns. While there is evidence of buoyancy-forced subsurface adjustment in the equatorial temperature profile, we highlight this additional surface pathway which can maintain the quasi-equilibrium response. We note, however, that we perform these experiments with CESM only and there may be model dependencies on surface and subsurface pathways and their timescales.

We highlight the utility of wind stress locking to predict the phase of equatorial mode responses to anomalous interannual to decadal forcing. These methods could be employed to understand the tropical Indo-Pacific SST quasi-equilibrium response to climate change and any subsequent downstream effects on global climate variability due to teleconnections between the tropical Pacific and the extratropics. While CESM seems to be an outlier in the strength of its atmosphere-ocean coupling, and thus its positive feedback strength, this pathway of three positive feedbacks seems to be somewhat robust across ETINMIP member models and is suggestive of a conduit connecting sustained extratropical forcing to tropical variability.

Data Availability Statement

The data used to create Figures 1 and 2 of this study and originally presented in Luongo et al. (2022) are publically available through the University of California, San Diego (UCSD) library digital collections: https://doi.org/10.6075/J05X294K. The wind stress overriding protocol for CESM is available on MTL's Github page and through the UCSD library digital collections: https://doi.org/10.6075/J09P31TF. The ETINMIP TOA insolation reduction CESM code and the long-term ETINMIP data used to create Figure 3 may be requested from the authors of Kang et al. (2019).

Acknowledgments
This work was supported by NSF Grants 2048590 and 1934392. In addition, MTL is supported by a NASA FINESST Fellowship (80NSSC22K1528). We thank UCAR and NSF for providing the graduate student allocation of core hours on Cheyenne that this research used and the ETINMIP group for making their NEXT experimental code and restart files available. Without implying their endorsement, we thank Shantong Sun, Mark England, and Qihua Peng for helpful discussions and suggestions. We also thank our editor, Dr. Kris Karnauskas, and two anonymous reviewers for their thoughtful and constructive feedback, which greatly improved this manuscript.

References

Amaya, D. J. (2019). The Pacific meridional mode and ENSO: A review. *Current Climate Change Reports*, *5*(4), 296–307. https://doi.org/10.1007/s40641-019-00142-x

Bjerknes, J. (1969). Atmospheric teleconnections from the equatorial Pacific. *Monthly Weather Revie*w, *97*(3), 163–172. https://doi.org/10.1175/1520-0493(1969)097<0163:atftep>2.3.co;2

Bunge, L., & Clarke, A. J. (2014). On the warm water volume and its changing relationship with ENSO. *Journal of Physical Oceanography*, *44*(5), 1372–1385. https://doi.org/10.1175/jpo-d-13-062.1

Burls, N. J., & Fedorov, A. V. (2014). What controls the mean east–west sea surface temperature gradient in the equatorial Pacific: The role of cloud albedo. *Journal of Climate*, *27*(7), 2757–2778. https://doi.org/10.1175/jcli-d-13-00255.1

Burls, N. J., Muir, L., Vincent, E. M., & Fedorov, A. (2017). Extra-tropical origin of equatorial Pacific cold bias in climate models with links to cloud albedo. *Climate Dynamics*, *49*(5), 2093–2113. https://doi.org/10.1007/s00382-016-3435-6

Chang, P., Zhang, L., Saravanan, R., Vimont, D. J., Chiang, J. C., Ji, L., et al. (2007). Pacific meridional mode and El Niño—Southern oscillation. *Geophysical Research Letters*, *34*(16), L16608. https://doi.org/10.1029/2007gl030302

Chiang, J. C., & Bitz, C. M. (2005). Influence of high latitude ice cover on the marine Intertropical Convergence Zone. *Climate Dynamics*, *25*(5), 477–496. https://doi.org/10.1007/s00382-005-0040-5

Chiang, J. C., & Vimont, D. J. (2004). Analogous Pacific and Atlantic meridional modes of tropical atmosphere–ocean variability. *Journal of Climate*, *17*(21), 4143–4158. https://doi.org/10.1175/jcli4953.1

Clement, A. C., Burgman, R., & Norris, J. R. (2009). Observational and model evidence for positive low-level cloud feedback. *Science*, *325*(5939), 460–464. https://doi.org/10.1126/science.1171255

Clement, A. C., Seager, R., Cane, M. A., & Zebiak, S. E. (1996). An ocean dynamical thermostat. *Journal of Climate*, 9(9), 2190–2196. https://doi.org/10.1175/1520-0442(1996)009<2190:aodt>2.0.co;2

Dong, B.-W., & Sutton, R. (2002). Adjustment of the coupled ocean–atmosphere system to a sudden change in the thermohaline circulation. *Geophysical Research Letters*, *29*(15), 18–21. https://doi.org/10.1029/2002gl015229

England, M. R., Polvani, L. M., Sun, L., & Deser, C. (2020). Tropical climate responses to projected Arctic and Antarctic sea-ice loss. *Nature Geoscience*, *13*(4), 275–281. https://doi.org/10.1038/s41561-020-0546-9

Erfani, E., & Burls, N. J. (2019). The strength of low-cloud feedbacks and tropical climate: A CESM sensitivity study. *Journal of Climate*, *32*(9), 2497–2516. https://doi.org/10.1175/jcli-d-18-0551.1

Forster, P., Storelvmo, T., Armour, K., Collins, W., Dufresne, J.-L., Frame, D., et al. (2021). The Earth's energy budget, climate feedbacks, and climate sensitivity. In *Climate change 2021: The physical science basis. Contribution of working group I to the sixth assessment report of the intergovernmental panel on climate change*. Cambridge University Press.

Green, B., & Marshall, J. (2017). Coupling of trade winds with ocean circulation damps ITCZ shifts. *Journal of Climate*, *30*(12), 4395–4411. https://doi.org/10.1175/jcli-d-16-0818.1

Gregory, J. M., Bouttes, N., Griffies, S. M., Haak, H., Hurlin, W. J., Jungclaus, J., et al. (2016). The flux-anomaly-forced model intercomparison project (FAFMIP) contribution to CMIP6: Investigation of sea-level and ocean climate change in response to CO_2 forcing. *Geoscientific Model Development*, *9*(11), 3993–4017. https://doi.org/10.5194/gmd-9-3993-2016

Hasselmann, K. (1976). Stochastic climate models part I. Theory. *Tellus*, *28*(6), 473–485. https://doi.org/10.1111/j.2153-3490.1976.tb00696.x

Heede, U. K., & Fedorov, A. V. (2021). Eastern equatorial Pacific warming delayed by aerosols and thermostat response to CO_2 increase. *Nature Climate Change*, *11*(8), 696–703. https://doi.org/10.1038/s41558-021-01101-x

Heede, U. K., Fedorov, A. V., & Burls, N. J. (2020). Time scales and mechanisms for the tropical Pacific response to global warming: A tug of war between the ocean thermostat and weaker Walker. *Journal of Climate*, *33*(14), 6101–6118. https://doi.org/10.1175/jcli-d-19-0690.1

Hsiao, W.-T., Hwang, Y.-T., Chen, Y.-J., & Kang, S. M. (2022). The role of clouds in shaping tropical Pacific response pattern to extratropical thermal forcing. *Geophysical Research Letters*, *49*(11), e2022GL098023. https://doi.org/10.1029/2022gl098023

Hurrell, J. W., Holland, M. M., Gent, P. R., Ghan, S., Kay, J. E., Kushner, P. J., et al. (2013). The community Earth system model: A framework for collaborative research. *Bulletin of the American Meteorological Society*, *94*(9), 1339–1360. https://doi.org/10.1175/bams-d-12-00121.1

Hwang, Y.-T., Xie, S.-P., Deser, C., & Kang, S. M. (2017). Connecting tropical climate change with Southern Ocean heat uptake. *Geophysical Research Letters*, *44*(18), 9449–9457. https://doi.org/10.1002/2017gl074972

Kang, S. M., Frierson, D. M., & Held, I. M. (2009). The tropical response to extratropical thermal forcing in an idealized GCM: The importance of radiative feedbacks and convective parameterization. *Journal of the Atmospheric Sciences*, *66*(9), 2812–2827. https://doi.org/10.1175/2009jas2924.1

Kang, S. M., Hawcroft, M., Xiang, B., Hwang, Y.-T., Cazes, G., Codron, F., et al. (2019). Extratropical–tropical interaction model intercomparison project (ETIN-MIP): Protocol and initial results. *Bulletin of the American Meteorological Society*, *100*(12), 2589–2606. https://doi.org/10.1175/BAMS-D-18-0301.1

Kang, S. M., Held, I. M., Frierson, D. M., & Zhao, M. (2008). The response of the ITCZ to extratropical thermal forcing: Idealized slab-ocean experiments with a GCM. *Journal of Climate*, *21*(14), 3521–3532. https://doi.org/10.1175/2007jcli2146.1

Kang, S. M., Held, I. M., & Xie, S.-P. (2014). Contrasting the tropical responses to zonally asymmetric extratropical and tropical thermal forcing. *Climate Dynamics*, *42*(7), 2033–2043. https://doi.org/10.1007/s00382-013-1863-0

Kang, S. M., Shin, Y., & Xie, S.-P. (2018). Extratropical forcing and tropical rainfall distribution: Energetics framework and ocean Ekman advection. *NPJ Climate and Atmospheric Science*, *1*(1), 20172. https://doi.org/10.1038/s41612-017-0004-6

Kang, S. M., Xie, S.-P., Shin, Y., Kim, H., Hwang, Y.-T., Stuecker, M. F., et al. (2020). Walker circulation response to extratropical radiative forcing. *Science Advances*, *6*(47), eabd3021. https://doi.org/10.1126/sciadv.abd3021

Kay, J. E., Deser, C., Phillips, A., Mai, A., Hannay, C., Strand, G., et al. (2015). The Community Earth System Model (CESM) large ensemble project: A community resource for studying climate change in the presence of internal climate variability. *Bulletin of the American Meteorological Society*, *96*(8), 1333–1349. https://doi.org/10.1175/bams-d-13-00255.1

Larson, S. M., & Kirtman, B. (2013). The Pacific meridional mode as a trigger for ENSO in a high-resolution coupled model. *Geophysical Research Letters*, *40*(12), 3189–3194. https://doi.org/10.1002/grl.50571

Larson, S. M., & Kirtman, B. P. (2014). The Pacific meridional mode as an ENSO precursor and predictor in the North American multimodel ensemble. *Journal of Climate*, *27*(18), 7018–7032. https://doi.org/10.1175/jcli-d-14-00055.1

Larson, S. M., Vimont, D. J., Clement, A. C., & Kirtman, B. P. (2018). How momentum coupling affects SST variance and large-scale Pacific climate variability in CESM. *Journal of Climate*, *31*(7), 2927–2944. https://doi.org/10.1175/jcli-d-17-0645.1

Liu, W., Lu, J., & Xie, S.-P. (2015). Understanding the Indian Ocean response to double CO_2 forcing in a coupled model. *Ocean Dynamics*, *65*(7), 1037–1046. https://doi.org/10.1007/s10236-015-0854-6

Liu, W., Lu, J., Xie, S.-P., & Fedorov, A. (2018). Southern Ocean heat uptake, redistribution, and storage in a warming climate: The role of meridional overturning circulation. *Journal of Climate*, *31*(12), 4727–4743. https://doi.org/10.1175/jcli-d-17-0761.1

Liu, Z. (1994). A simple model of the mass exchange between the subtropical and tropical ocean. *Journal of Physical Oceanography*, *24*(6), 1153–1165. https://doi.org/10.1175/1520-0485(1994)024<1153:asmotm>2.0.co;2

Liu, Z., & Huang, B. (1997). A coupled theory of tropical climatology: Warm pool, cold tongue, and Walker circulation. *Journal of Climate*, *10*(7), 1662–1679. https://doi.org/10.1175/1520-0442(1997)010<1662:actotc>2.0.co;2

Lu, F., Liu, Z., Liu, Y., Zhang, S., & Jacob, R. (2017). Understanding the control of extratropical atmospheric variability on ENSO using a coupled data assimilation approach. *Climate Dynamics*, *48*(9–10), 3139–3160. https://doi.org/10.1007/s00382-016-3256-7

Luongo, M. T., Xie, S.-P., & Eisenman, I. (2022). Buoyancy forcing dominates the cross-equatorial ocean heat transport response to northern hemisphere extratropical cooling. *Journal of Climate*, *35*(20), 3071–3090. https://doi.org/10.1175/jcli-d-21-0950.1

Ma, J., Xie, S.-P., & Xu, H. (2017). Contributions of the North Pacific meridional mode to ensemble spread of ENSO prediction. *Journal of Climate*, *30*(22), 9167–9181. https://doi.org/10.1175/jcli-d-17-0182.1

Mahajan, S., Saravanan, R., & Chang, P. (2009). The role of the wind-evaporation-sea surface temperature (WES) feedback in air–sea coupled tropical variability. *Atmospheric Research*, *94*(1), 19–36. https://doi.org/10.1016/j.atmosres.2008.09.017

Mahajan, S., Saravanan, R., & Chang, P. (2011). The role of the wind–evaporation–sea surface temperature (WES) feedback as a thermodynamic pathway for the equatorward propagation of high-latitude sea ice–induced cold anomalies. *Journal of Climate*, *24*(5), 1350–1361. https://doi.org/10.1175/2010jcli3455.1

McCreary, J. P., & Lu, P. (1994). Interaction between the subtropical and equatorial ocean circulations: The subtropical cell. *Journal of Physical Oceanography*, *24*(2), 466–497.

Meinen, C. S., & McPhaden, M. J. (2000). Observations of warm water volume changes in the equatorial Pacific and their relationship to El Niño and La Niña. *Journal of Climate*, *13*(20), 3551–3559. https://doi.org/10.1175/1520-0442(2000)013<3551:oowwvc>2.0.co;2

Nonaka, M., Xie, S.-P., & McCreary, J. P. (2002). Decadal variations in the subtropical cells and equatorial Pacific SST. *Geophysical Research Letters*, *29*(7), 20–21. https://doi.org/10.1029/2001gl013717

Nonaka, M., Xie, S.-P., & Takeuchi, K. (2000). Equatorward spreading of a passive tracer with application to North Pacific interdecadal temperature variations. *Journal of Oceanography*, *56*(2), 173–183. https://doi.org/10.1023/a:1011135113079

Norris, J. R., & Leovy, C. B. (1994). Interannual variability in stratiform cloudiness and sea surface temperature. *Journal of Climate*, *7*(12), 1915–1925. https://doi.org/10.1175/1520-0442(1994)007<1915:ivisca>2.0.co;2

Norris, J. R., Zhang, Y., & Wallace, J. M. (1998). Role of low clouds in summertime atmosphere–ocean interactions over the North Pacific. *Journal of Climate*, *11*(10), 2482–2490. https://doi.org/10.1175/1520-0442(1998)011<2482:rolcis>2.0.co;2

Pegion, K. V., & Selman, C. (2017). Extratropical precursors of the El Niño–Southern Oscillation. *Climate Extremes: Patterns and Mechanisms*, *226*, 301.

Richter, I., & Xie, S.-P. (2008). On the origin of equatorial Atlantic biases in coupled general circulation models. *Climate Dynamics*, *31*(5), 587–598. https://doi.org/10.1007/s00382-008-0364-z

Richter, I., Xie, S.-P., Wittenberg, A. T., & Masumoto, Y. (2012). Tropical Atlantic biases and their relation to surface wind stress and terrestrial precipitation. *Climate Dynamics*, *38*(5), 985–1001. https://doi.org/10.1007/s00382-011-1038-9

Smirnov, D., & Vimont, D. J. (2012). Extratropical forcing of tropical Atlantic variability during boreal summer and fall. *Journal of Climate*, *25*(6), 2056–2076. https://doi.org/10.1175/jcli-d-11-00104.1

Stuecker, M. F., Timmermann, A., Jin, F.-F., Proistosescu, C., Kang, S. M., Kim, D., et al. (2020). Strong remote control of future equatorial warming by off-equatorial forcing. *Nature Climate Change*, *10*(2), 124–129. https://doi.org/10.1038/s41558-019-0667-6

Thomas, E. E., & Vimont, D. J. (2016). Modeling the mechanisms of linear and nonlinear ENSO responses to the Pacific meridional mode. *Journal of Climate*, *29*(24), 8745–8761. https://doi.org/10.1175/jcli-d-16-0090.1

Thomas, M. D., & Fedorov, A. V. (2017). The eastern subtropical Pacific origin of the equatorial cold bias in climate models: A Lagrangian perspective. *Journal of Climate*, *30*(15), 5885–5900. https://doi.org/10.1175/jcli-d-16-0819.1

Vannière, B., Guilyardi, E., Toniazzo, T., Madec, G., & Woolnough, S. (2014). A systematic approach to identify the sources of tropical SST errors in coupled models using the adjustment of initialized experiments. *Climate Dynamics*, *43*(7), 2261–2282. https://doi.org/10.1007/s00382-014-2051-6

Verma, T., Saravanan, R., Chang, P., & Mahajan, S. (2019). Tropical Pacific Ocean dynamical response to short-term sulfate aerosol forcing. *Journal of Climate*, *32*(23), 8205–8221. https://doi.org/10.1175/jcli-d-19-0050.1

Vimont, D. J., Wallace, J. M., & Battisti, D. S. (2003). The seasonal footprinting mechanism in the Pacific: Implications for ENSO. *Journal of Climate*, *16*(16), 2668–2675. https://doi.org/10.1175/1520-0442(2003)016<2668:tsfmit>2.0.co;2

Wang, K., Deser, C., Sun, L., & Tomas, R. A. (2018). Fast response of the tropics to an abrupt loss of Arctic sea ice via ocean dynamics. *Geophysical Research Letters*, *45*(9), 4264–4272. https://doi.org/10.1029/2018gl077325

Wood, R. (2012). Stratocumulus clouds. *Monthly Weather Review*, *140*(8), 2373–2423. https://doi.org/10.1175/mwr-d-11-00121.1

Wyrtki, K. (1975). El Niño—the dynamic response of the equatorial Pacific Ocean to atmospheric forcing. *Journal of Physical Oceanography*, *5*(4), 572–584. https://doi.org/10.1175/1520-0485(1975)005<0572:entdro>2.0.co;2

Xie, S.-P. (1999). A dynamic ocean–atmosphere model of the tropical Atlantic decadal variability. *Journal of Climate*, *12*(1), 64–70. https://doi.org/10.1175/1520-0442-12.1.64

Xie, S.-P., Deser, C., Vecchi, G. A., Ma, J., Teng, H., & Wittenberg, A. T. (2010). Global warming pattern formation: Sea surface temperature and rainfall. *Journal of Climate*, *23*(4), 966–986. https://doi.org/10.1175/2009jcli3329.1

Xie, S.-P., & Philander, S. G. H. (1994). A coupled ocean-atmosphere model of relevance to the ITCZ in the eastern Pacific. *Tellus A*, *46*(4), 340–350. https://doi.org/10.3402/tellusa.v46i4.15484

Yang, L., Xie, S.-P., Shen, S. S., Liu, J.-W., & Hwang, Y.-T. (2022). Low cloud-SST feedback over the subtropical northeast Pacific and the remote effect on ENSO variability. *Journal of Climate*, 1–28.

Yoshimori, M., & Broccoli, A. J. (2008). Equilibrium response of an atmosphere–mixed layer ocean model to different radiative forcing agents: Global and zonal mean response. *Journal of Climate*, *21*(17), 4399–4423. https://doi.org/10.1175/2008jcli2172.1

Yu, S., & Pritchard, M. S. (2019). A strong role for the AMOC in partitioning global energy transport and shifting ITCZ position in response to latitudinally discrete solar forcing in CESM1. 2. *Journal of Climate*, *32*(8), 2207–2226. https://doi.org/10.1175/jcli-d-18-0360.1

Zelinka, M. D., Myers, T. A., McCoy, D. T., Po-Chedley, S., Caldwell, P. M., Ceppi, P., et al. (2020). Causes of higher climate sensitivity in CMIP6 models. *Geophysical Research Letters*, *47*(1), e2019GL085782. https://doi.org/10.1029/2019gl085782

Zhang, R., & Delworth, T. L. (2005). Simulated tropical response to a substantial weakening of the Atlantic thermohaline circulation. *Journal of Climate*, *18*(12), 1853–1860. https://doi.org/10.1175/jcli3460.1

Zhang, Y., Yu, S., Amaya, D. J., Kosaka, Y., Larson, S. M., Wang, X., et al. (2021). Pacific meridional modes without equatorial Pacific influence. *Journal of Climate*, *34*(13), 5285–5301. https://doi.org/10.1175/jcli-d-20-0573.1